Identity of planar defects in the 'infinite-layer' copper oxide superconductor

H. Zhang*, Y. Y. Wang*, H. Zhang*, V. P. Dravid*†, L. D. Marks*, P. D. Han‡, D. A. Payne‡, P. G. Radaelli§ & J. D. Jorgensen§

Science and Technology Center for Superconductivity:
* Department of Materials Science and Engineering, Northwestern University, Evanston, Illinois 60208, USA
‡ Department of Materials Science and Engineering, University of Illinois at Urbana-Champaign, Urbana, Illinois 61801, USA
§ Materials Science Division, Argonne National Laboratory, Argonne, Illinois 60439, USA

THE 'infinite-layer' compound[1–3] $ACuO_2$ (where A stands for cations such as strontium or calcium), has the simplest structure of all superconducting copper oxides, with only bare cations separating the CuO_2 planes. Accordingly, an understanding of the doping mechanism(s) that lead to superconductivity in this compound may facilitate the elucidation of the same phenomenon in the other copper oxide superconductors. Recently, Azuma and co-workers[2,4] observed planar defects in an infinite-layer phase synthesized at high oxygen pressure, and proposed that the defects are A-cation deficient, and lead to superconductivity (with transition temperature $T_C \approx 100$–110 K) in this compound. Here, based on quantitative X-ray and high-resolution electron-microscopic analysis of the planar defects in (Sr, Ca)CuO_2, we propose that the defects consist of a corrugated Sr–O layer substituted for a CuO_2 layer, with the incorporation of apical oxygen atoms (which are absent in the parent structure) at roughly half the available sites in the neighbouring Sr layers. This is equivalent to an insertion of a Sr_3O_{2+x} block in an otherwise infinite-layer sequence. The variable oxygen stoichiometry of our defect model can account for the occurrence of p-type superconductivity (following high-pressure oxygenation), n-type superconductivity (high-pressure reduction) or lack of superconductivity (high-pressure neutral-atmosphere annealing) in this system, depending on the synthesis conditions[4].

Infinite-layer samples with the nominal chemical formula $(Sr_{1-x}Ca_x)_yCuO_2$ ($y = 0.9$, 1.0 and 1.1; $x = 0.3$) were prepared using pre-synthesized precursors of low-pressure forms of $(Sr_{1-x}Ca_x)CuO_2$ with additions of CuO and $(Sr_{1-x}Ca_x)_2CuO_3$, followed by a high-pressure treatment. The synthesis conditions were 6 GPa oxidizing pressure at 1,050 °C for 1 h. The oxidizing pressure was created in a classical piston-cylinder press by decomposition of $KClO_4$, which sandwiched the sample pellet; the 'sandwich' was contained in a gold capsule. All the compositions exhibited an onset of superconductivity above 100 K with varying Meissner fractions. (We have since synthesized a superconducting infinite-layer compound without calcium (that is, just $SrCuO_2$) but the synthesis conditions are not yet optimized for high Meissner fraction.)

Neutron and X-ray powder diffraction data showed that the dominant phase was the infinite-layer structure, with peak broadening characteristic of planar defects. No other phases known to be superconducting were seen. In particular, there was no evidence of $Sr_{n+1}Cu_nO_{2n+1+x}$-type phases, which are formed under similar high-pressure conditions and can have T_cs near 100 K (refs 5, 6).

High-spatial-resolution X-ray microanalysis was performed using a cold field-emission gun transmission electron microscope (Hitachi HF-2000) equipped with an Oxford Pentafet thin-window X-ray detector[7]. A probe size of ~1 nm full-width half-maximum (FWHM) was positioned on the planar defects, and X-ray emission spectra from these regions were compared with those obtained from defect-free regions. In all cases, care was taken to account for spurious signals, counting statistics and appropriate Student's t-test error analysis[7].

Dedicated imaging was performed using a Hitachi H-9000 high-resolution electron microscope (HREM). Initially, the high-resolution images were compared visually to simulated ones using two multislice routines (NUMIS (L. D. Marks, Northwestern University, USA) and the MacTempas suite of programs (Total Resolution, Berkeley, USA)) as a function of objective lens defocus and specimen thickness. A second more careful set of experimental images were then obtained, digitized and compared quantitatively with calculated images. Briefly, the standard deviations of the experimental data were obtained from the cell-to-cell variations, and these values used for conventional χ^2 fittings (where χ^2 is defined as the total sum of the square of the difference between the experimental and simulated value for each pixel; the reduced χ^2 is normalized by the number of the data points). The electron-optical conditions were determined by fitting the matrix, and these same conditions were used for the defect structure. The atomic positions of the defect structure were determined by minimizing the χ^2 error.

The planar defects that we observed in our sample are virtually identical in terms of appearance, contrast, form and distribution to those reported earlier[2,4]. Some of the planar defects do not extend indefinitely in the x–y plane, but gradually disappear in the bulk crystal. The defect density varies from region to region. The X-ray microanalysis results (Fig. 1) with a 1-nm probe show an excess (Sr + Ca)/Cu X-ray signal from the planar-defect regions. A notable decrease in the Ca signal in the defect region was observed, but overall, there was an enrichment of the A-cation (Sr + Ca) relative to Cu in the defect region. The composition of the defect region (which includes some non-defective material because of beam broadening) was calculated using the non-defective region as an internal standard. Relative to the non-defective region, there was an excess of ~32% Sr/Cu atomic ratio, depletion of ~27% Ca/Cu atomic ratio, but excess of ~16% A-cation (Sr + Ca) over Cu on the planar defect. X-ray beam-broadening calculations and Monte Carlo simulations[8] indicated that the excess of A-cation to Cu translates into substitution of a single layer of Sr (and some O) for a Cu layer, and considerable depletion of Ca in the defect region, such that the overall chemistry of the defect region is cation-rich. In addition to the nanoprobe analysis, a larger probe (~50–100 nm FWHM) was positioned in areas containing closely spaced (~2–5 nm)

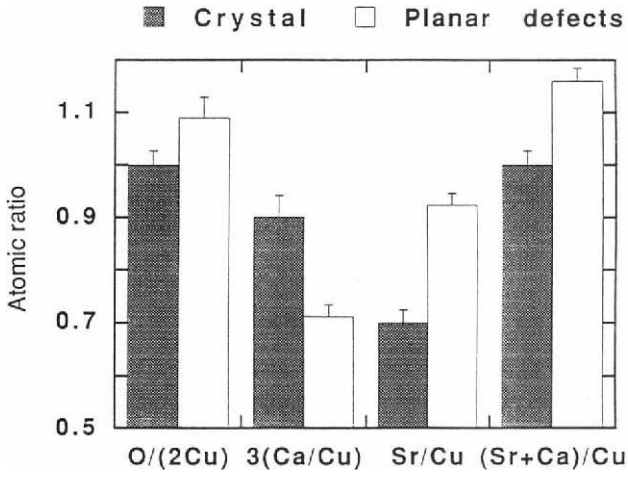

FIG. 1 Energy dispersive X-ray analysis of planar defects and perfect crystal with ~1-nm electron probe. Error bars show the standard error of the mean, determined from 10 sets of measurements both on and off the planar defects.

† To whom correspondence should be addressed.

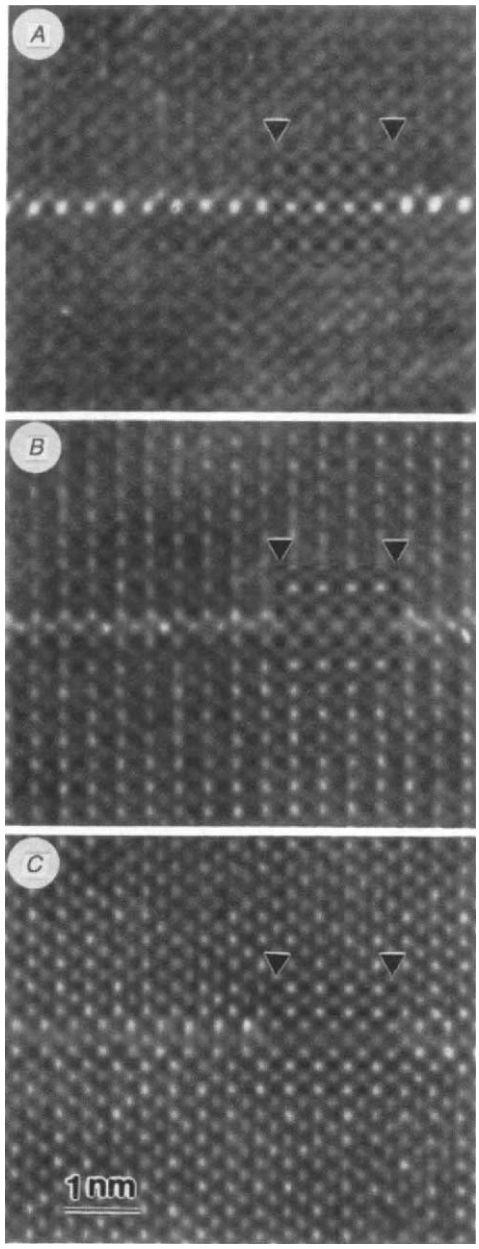

FIG. 2 Comparison of experimental and simulated HREM images of planar defects in the infinite-layer compound as a function of objective lens defocus. The defocus distances are 0, −440 and −740 Å for panels *A*, *B* and *C*, respectively, with a sample thickness of 20 Å. The reduced χ^2 values are 2.01 (*A*), 1.72 (*B*) and 1.66 (*C*).

planar defects, and the X-ray data compared with that obtained with the same probe size in defect-free regions. Consistent excess of (Sr + Ca) over Cu in the defect-rich region was also observed in these experiments. These results contradict the A-cation deficiency model proposed by Hiroi *et al.*[2,4].

Exploiting the X-ray microanalysis results, a large number of different structural models were tested against experimental HREM images. Figure 2 shows three images. Analysis of the images indicates that changes need to be made both in the CuO_2 plane and in the Sr planes above and below the defect layer. Simply substituting Sr for Cu for this plane and/or introducing O vacancies did not reproduce the experimental images. We also tested the cation-deficiency model proposed by Hiroi *et al.*[4] and reached the same conclusion: our simulated images of their model deviate strongly from our high-resolution images as well as theirs.

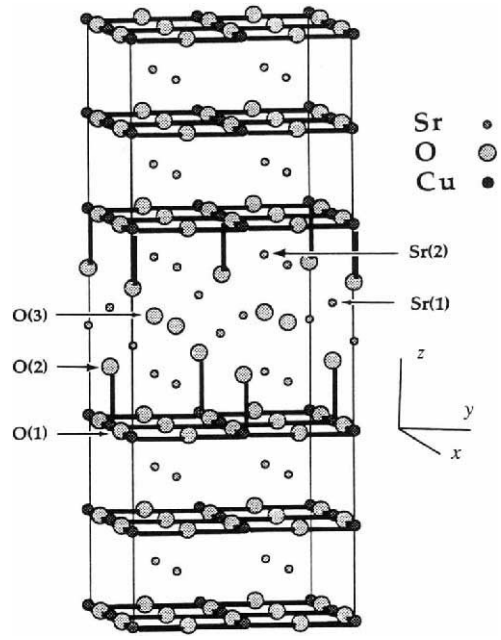

FIG. 3 The structural model for the planar defects, two unit cells wide along *x* and *y* directions. Three Sr–O layers replace a Sr–CuO_2–Sr block in an otherwise perfect infinite-layer structure. The ordering in the figure is shown only for convenience and to aid the eye.

The structural model that matches all the experimental HREM images is shown in Fig. 3. The reduced χ^2 values are 2.01, 1.72 and 1.66 for defoci of 0, −440 and −740 Å, respectively, as shown in Fig. 2*A*, *B* and *C*. This model is A-cation (Sr) rich, with the substitution of a corrugated Sr–O layer for a CuO layer, and the incorporation of oxygen at roughly half the available sites in the neighbouring Sr layers (that is, substitution of an $Sr_3O_{2\pm x}$ block for a Sr–CuO_2–Sr block in an otherwise infinite-layer structure sequence). The middle layer consists of a stoichiometric Sr(1)–O(3) sheet, whereas the two outer Sr–O layers, which contain Sr(2) and O(2), have ~50% occupancy of O(2). The Sr(1) atoms are not coplanar with the O(3) atoms, but are staggered up or down from the centre of the unit cell by $0.58 \pm 0.07(\sigma)$ Å along the *c*-axis (the mean and error for vertical staggering are calculated based on fitting data from three defocus measurements). Because HREM images or diffraction patterns taken along other zone axes (for example, [110]) did not show any higher-order periodicity for the defects, we assumed random occupancy for Sr(1): in other words, the sign of the staggering (above or below the centre of the unit cell) of Sr(1), and thus that of O(2), may vary. The distance from the centre of the planar defect to the neighbouring CuO_2 planes (through a Sr(2)–O(2) layer) is increased from 3.4 Å to ~3.7 Å, in agreement with the previous observations[4].

Based on charge-neutrality arguments, about half of the possible sites for O(2) contain oxygen, leading to apical oxygen atoms for about half of the Cu atoms in the adjacent CuO_2 planes, located along the longer Sr(1)-Cu bond. For the Sr(2) position, the simulation indicates that the Sr(2) atom is $1.5 \pm 0.1(\sigma)$ Å away from the nearest CuO_2 plane. The Sr–O distances are; Sr(1)–O(2) = 2.13 Å, Sr(1)–O(3) = 2.82 Å, Sr(2)–O(2) = 2.84 Å and Sr(2)–O(3) = 2.22 Å. The atomic positions for the defects are listed in Table 1.

Our model for the planar defects is a configuration not yet seen in any layered copper oxide compounds made under abient conditions. The similarity to the Sr_2O_{1+x} layers in the newly discovered $Sr_{n+1}Cu_nO_{2n+1+x}$ compounds[9,10] which are also synthesized at higher pressure, is intriguing. Hirol *et al.*[9,10] have speculated that high pressure reduces the mismatch between the

TABLE I Atomic positions for the planar defect compared to those for the non-defective infinite-layer unit cell

Planar defect atomic positions				Corresponding non-defective infinite-layer atomic positions			
Atom	x	y	z	Atom	x	y	z
Cu	0	0	0	Cu	0	0	0
O(1)	0.5	0	0	O	0.5	0	0
O(1)	0	0.5	0	O	0	0.5	0
O(2)*	0	0	0.29	O†	–	–	–
O(2)*	0	0	0.71	O†	–	–	–
				O	0.5	0	0.5
O(3)	0.5	0.5	0.5				
				O	0	0.5	0.5
Sr(1)*	0	0	0.422				
				Cu	0	0	0.5
Sr(1)*	0	0	0.578				
Sr(2)	0.5	0.5	0.20	Sr	0.5	0.5	0.25
Sr(2)	0.5	0.5	0.80	Sr	0.5	0.5	0.75

The unit cell for the defect is $3.9 \times 3.9 \times 7.4$ Å (x, y, z), while that for the non-defective infinite-layer compound is: $3.9 \times 3.9 \times 6.8$ Å (x, y, (2)z). The atomic positions are scaled to the unit-cell length. The staggering of Sr(1) is 0.078 times the unit-cell length along c-axis, which results in Sr(1) positions being, $0.50 - 0.078 = 0.422$ and $0.50 + 0.078 = 0.578$.

* Half occupancy.

† No apical oxygens.

CuO_2 and Sr–O layers, allowing new structures to form. The triple Sr–O layer model can than be thought of as an extension of the double Sr layers present in $Sr_{n+1}Cu_nO_{2n+1+x}$ compounds. We have not seen any defects with more than three layers in these compounds. While other known hole-doped copper oxide superconductors have a homogeneous occupancy of apical oxygen sites there are no apical oxygen atoms in the non-defective infinite-layer compound. It appears that the planar defects provide at least half of the possible number of the apical oxygens to the CuO_2 planes and therefore permit hole-doped high-T_c superconductivity. (The previously proposed[10] half-occupancy of apical oxygen sites in Sr_2CuO_3 has been called into question by recent neutron-diffraction experiments.[11])

It should be pointed out that neither X-ray microanalysis nor HREM imaging can define the oxygen content and locations precisely. The two Sr positions (both Sr(1) and Sr(2)) are determined here with a high degree of confidence, but the O positions are assigned according to the cation positions. Because the cation position is dictated by anion coordination, the observed staggering of Sr(1) is clearly due to the reduction of apical oxygen occupancy, which is also consistent with the charge neutrality arguments.

We speculate that these planar defects can be p-type if doped by excess oxygen ($x > 0$) or n-type with oxygen deficiency ($x < 0$), leading to both p- and n-type superconductivity. Furthermore, for $x = 0$, one can obtain neutral Sr_3O_2 layers. This hypothesis agrees with previous observations of superconductivity in this system[4] as a function of the synthesis atmosphere, that is p-type with $T_c \approx 110$ K under oxidizing conditions and n-type with $T_c \approx 43$ K under reducing conditions.

We have found that compositions with excess cation ($y > 1$) show an increased Meissner fraction by a factor of almost four, relative to the stoichiometric or $y < 1$ compositions. This is consistent with A-cation-rich planar defects observed in this study. In our most recent experiments on pure $SrCuO_2$ (that is, no calcium), we also observe planar defects similar to those reported here and they too are Sr-rich. □

Received 8 April; accepted 28 June 1994.

1. Siegrist, T., Zahurak, S. M., Murphy, D. W. & Roth, R. S. *Nature* **334,** 231–232 (1988).
2. Azuma, M., Hiroi, Z., Takano, M., Bando, Y. & Takeda, Y. *Nature* **356,** 775–776 (1992).
3. Jorgensen, J. D., Radaelli, P. G., Hinks, D. G. & Wagner, J. L. *Phys. Rev.* B**47,** 14654–14656 (1993).
4. Hiroi, Z., Azuma, M., Takano, M. & Takeda, Y. *Physica* C**208,** 286–196 (1993).
5. Adachi, S., Yamauchi, H., Tanaka, S. & Mori, N. *Physica* C**208,** 226–230 (1993).
6. Radaelli, P. G. & Jorgensen, J. D. *Nature* **364,** 286–287 (1993).
7. Dravid, V. P., Zhang, H., Zhang, J. P. & Marks, L. D. *Physica* C**192,** 31–34 (1992).
8. Principles of Analytical Electron Microscopy (eds Joy, D. C., Romig, A. Jr & Goldstein, J. I.) Ch. 4 & 5 (Plenum, New York, 1986).
9. Adachi, S., Yamauchi, H., Tanaka, S. & Mori, N. *Physica* C**212,** 164–168 (1993).
10. Hiroi, Z., Azuma, M., Takano, M. & Takeda, Y. *Nature* **364,** 315–317 (1993).
11. Shimakawa, Y. *et al. Physica* C. (in the press).

ACKNOWLEDGEMENTS. The research was supported by the NSF US through the Science and Technology Center for Superconductivity (STCS) and the US Department of Energy.

Light-emitting diodes made from cadmium selenide nanocrystals and a semiconducting polymer

V. L. Colvin, M. C. Schlamp & A. P. Alivisatos

Materials Sciences Division, Lawrence Berkeley Laboratory, and Department of Chemistry, University of California at Berkeley, Berkeley, California 94720, USA

ELECTROLUMINESCENT devices have been developed recently that are based on new materials such as porous silicon[1] and semiconducting polymers[2,3]. By taking advantage of developments in the preparation and characterization of direct-gap semiconductor nanocrystals[4–6], and of electroluminescent polymers[7], we have now constructed a hybrid organic/inorganic electroluminescent device. Light emission arises from the recombination of holes injected into a layer of semiconducting *p*-paraphenylene vinylene (PPV)[8–10] with electrons injected into a multilayer film of cadmium selenide nanocrystals. Close matching of the emitting layer of nanocrystals with the work function of the metal contact leads to an operating voltage[11] of only 4 V. At low voltages emission from the CdSe layer occurs. Because of the quantum size effect[19–24] the colour of this emission can be varied from red to yellow by changing the nanocrystal size. At higher voltages green emission from the polymer layer predominates. Thus this device has a degree of voltage tunability of colour.

Nanocrystals normally exist as powders or dissolved in liquids. To employ them in devices it is necessary to develop new techniques of assembly which allow charge injection into, and transport through, nanocrystals. To achieve this goal we construct multilayers of nanocrystals using the well-developed chemistry of thiols on metal surfaces. Narrow size distributions (±5% of the diameter) of CdSe nanocrystals with absorption maxima in the range 580–620 nm (30–50 Å diameter) are prepared by the TOPO method of Murray and Bawendi[5] as modified by Bowen Katari *et al.*[6]. The nanocrystals are dissolved in toluene, and this solution is exposed to either bare indium tin oxide (ITO) or ITO/PPV plates which have been pretreated with hexane dithiol, a bifunctional compound that binds nanocrystals to surfaces[6,12]. This procedure is repeated five times, leading to the formation of a multilayer structure with closely packed disordered sheets of CdSe nanocrystals separated by organic spacers. This well-characterized buildup process permits the isolated nanocrystals to be investigated before being incorporated into the diode structure. In addition, this process permits nanocrystals with different electronic properties to be placed in defined locations in the same device. The overall thickness of the nanocrystal multilayer is only a few hundred ångströms. This thin layer readily undergoes dielectric breakdown at the voltages required for operation. For this reason, a 1,000-Å-thick layer of PPV, prepared by standard methods (250 °C conversion temperature and absorption maximum at 415 nm), is a desirable